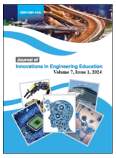

Journal of Innovations in Engineering Education
JIEE 2024, Vol. 7, Issue 1.

https://doi.org/10.3126/jiee.v7i1.66238

THAPATHALI CAMPUS
Institute of Engineering
Tribhuvan University

Modal analysis of multi-disk rotor system

Sunil Pradhan[a,*], Mahesh Chandra Luintel [a]

[a]*Institute of Engineering, Pulchowk Campus, Lalitpur*

ARTICLE INFO

Article history:

Received 26 August 2024
Revised in 1 October 2024
Accepted 15 October 2024

Keywords:

Dynamic analysis
ANSYS
Vibration
Campbell diagram
Natural frequency

Abstract

Vibration control is crucial for safe and effective operation of rotating machinery in industries such as aerospace, automotive, and power generation. This work studies the modal behavior of multi-disk rotor systems, a key field in mechanical engineering, utilizing a combination of analytical and mathematical models, as well as ANSYS-based simulations. The research uses ANSYS modal analysis to identify natural frequencies and mode shapes, with a focus on backward and forward spin frequencies. The results demonstrate that the first three natural frequencies for forward whirl under free response conditions are 67.155 Hz, 72.437 Hz, and 94.736 Hz, with a divergence of less from theoretical predictions, indicating that the mathematical model is accurate. Furthermore, the critical speed for the system's first mode of transverse vibration was determined to be 459.83 rad/s, which corresponds to important rotational velocities where considerable vibrations occur. This consistency of computational and analytical results emphasizes the vital need of identifying and regulating important frequencies to avoid operational breakdowns. The findings highlight the importance of precise modeling techniques in improving the dependability and performance of rotor systems, giving critical insights for the design and optimization of rotating machinery in a variety of industrial applications, resulting in increased safety and operational efficiency.

1. Introduction

In various engineering applications, such as power generation and machinery, the presence of rotating systems comprising disks attached to shafts is ubiquitous. Notably, these systems are integral components in the generation of power, both producing and consuming it [1]. Take, for instance, the Pelton turbine employed in hydropower plants, an emblematic example of a disk-shaft assembly. These turbines, serving across a spectrum from micro hydro to high-power plants, operate under harsh conditions. The challenge lies in enhancing their performance, longevity, and reducing weight without compromising reliability.

The primary concern within this context is the dynamic behavior of these rotating systems, which is crucial for their efficient and secure operation. To address this challenge, an exploration of dynamic behavior is essential. [2] Researchers have delved into various aspects of these systems, exploring the dynamic interplay between flexible and rigid components. They have examined flexible shafts modeled as Euler-Bernoulli beams, covering various modes of vibration, including bending, torsion, and longitudinal oscillations.

Similarly, the realm of rotating machinery encompasses a wide array of industries, including industrial, automotive, and aerospace. The operational efficiency of these systems is paramount for safety and effectiveness. Central to the issue of rotating machinery lies the dynamic behavior of rotor systems—comprising shafts and one or more disks. The presence of imbalanced masses in these systems can lead to disruptive vibrations and other dynamic challenges. These systems find applications in power generation through turbines, compressors, and pumps, where imbalanced mass-induced vibrations can compromise efficiency and accelerate wear and tear.[3]

Beyond power production, rotor systems with multiple disks and imbalanced masses play a vital role in various industrial applications, such as manufacturing machinery, wind turbines, and marine propulsion systems. [4] Controlling vibrations in these systems is critical, given their direct impact on dynamic behavior.

The complex interplay of components and operating

*Corresponding author:
pradhansunil737@gmail.com (S. Pradhan)

parameters influences the dynamic response of these shaft-disk systems. Past research efforts have undertaken diverse approaches to comprehend their behavior, with some assuming a flexible shaft and a rigid disk while others considered both shaft and disk flexibility. The bearings have also been a subject of investigation, with some studies focusing on rigid bearings and others on flexible ones.[5] Despite this extensive research, the dynamic behavior of rotor systems with multiple disks and uneven masses continues to be a fertile area for exploration. Numerous variables, such as system stiffness, mass distribution of disks, and the position of the imbalanced mass, collectively shape the system's dynamic response. [6] Comprehensive examination of these elements is necessary to truly understand the system's behavior and devise effective strategies for enhancing performance.

This thesis advocates for a comprehensive approach, utilizing analytical and mathematical modelling in tandem with ANSYS simulations, to dissect the dynamic behavior of rotor systems featuring multiple disks and imbalanced masses. This multi-pronged analysis promises valuable insights into the performance and reliability enhancement of these critical engineering components.

2. Development of mathematical modelling

2.1. Problem formulation using Euler-Bernoulli beam model

Consider a two rigid disk attached to a flexible shaft as shown in Figure 1, which is simply supported at the end by bearings. The axes x, y, and z are chosen such that x is along the longitudinal direction of the shaft, and y is along the transverse direction of the shaft on the vertical plane. Similarly, transverse displacements of any point of the shaft along horizontal and vertical directions are respectively v(x,t) and w(x,t). The shaft-rotor system is characterized by material properties Elasticity E, Density ρ, and Cross-sectional area A.

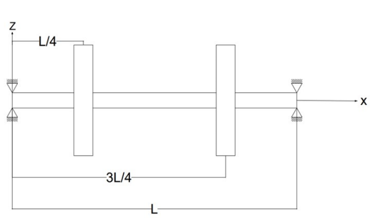

Figure 1: Diagram of the Shaft-disk assembly, illustrating the configuration of the flexible shaft connected to rigid disks.

2.2. System kinematics

A diagram illustrating a flexible shaft connected to a rigid disk in rotation is presented in the Figure 2. The shaft rotates around the x-axis at a consistent system x, y, z. The y and z axes also rotate at the same angular velocity Ω with respect to the x-axis, keeping pace with the rotating body. The deflection or bending of the shaft at any point along its neutral axis can be described as v (x, t) and w (x, t) along the y and z directions, respectively. The angular velocity vector and the neutral axis position vector can be written in vector form as follows:[7].

$$\boldsymbol{\omega}_s = [\Omega, 0, 0] \tag{1}$$

$$\boldsymbol{r}_s = v\mathbf{j} + w\mathbf{k} \tag{2}$$

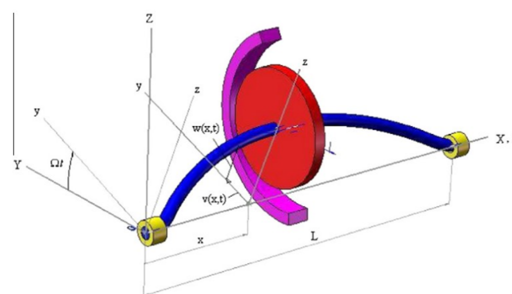

Figure 2: Rotating flexible Shaft-disk system in a deformed position [8]

The velocity of any point on the neutral axis of the shaft with reference to the inertial frame is given by: [8]

$$\boldsymbol{v}_s = \dot{v}\mathbf{j} + \dot{w}\mathbf{k} + \boldsymbol{\Omega}\times(v\mathbf{j} + w\mathbf{k}) = (\dot{v} - \Omega w)\mathbf{j} + (\dot{w} + \Omega v)\mathbf{k} \tag{3}$$

2.3. Kinetic and strain energy of rotating Shaft-disk System

The kinetic energy expression of a rotating shaft is given by: [1]

$$\begin{aligned} T_s = {} & \frac{1}{2}\rho A \int_0^L \left[(\dot{v} - \Omega w)^2 + (\dot{w} + \Omega v)^2\right] dx \\ & + \frac{1}{2}\rho J_p S \int_0^L (\Omega + v' \dot{w}')^2 \, dx \\ & + \frac{1}{2}\rho I_s \int_0^L \left[(-\Omega v' - \dot{w}')^2 + (-\Omega w' + \dot{v}')^2\right] dx \end{aligned} \tag{4}$$

Where ρ is the density, A is the cross-sectional area, L is the length of shaft, v and w are transverse displacements, and Ω is the angular velocity.

Avoiding the higher order terms, the Kinetic Energy of the shaft given by Equation (4) can be expressed as:

$$\begin{aligned}
T_s = &\frac{1}{2}\rho A \int_0^L \dot{v}^2\,dx + \frac{1}{2}\rho A \int_0^L \dot{w}^2\,dx \\
&+ \frac{1}{2}\rho A\Omega^2 \int_0^L v^2\,dx + \frac{1}{2}\rho A\Omega^2 \int_0^L w^2\,dx \\
&+ \rho A\Omega \int_0^L \dot{w}v\,dx - \rho A\Omega \int_0^L \dot{v}w\,dx + \frac{1}{2}\rho J_{ps}\Omega^2 L \\
&+ \rho J_{ps}\Omega \int_0^L \dot{w}'v'\,dx + \frac{1}{2}\rho I_s \int_0^L (\dot{v}')^2\,dx \\
&+ \frac{1}{2}\rho I_s \int_0^L (\dot{w}')^2\,dx + \frac{1}{2}\rho I_s\Omega^2 \int_0^L (v')^2\,dx \\
&+ \frac{1}{2}\rho I_s\Omega^2 \int_0^L (w')^2\,dx + \rho I_s\Omega \int_0^L \dot{w}'v'\,dx \\
&- \rho I_s\Omega \int_0^L \dot{v}'w'\,dx
\end{aligned} \tag{5}$$

Rigid disk's kinetic Energy expression takes the form,

$$\begin{aligned}
T_d = &\frac{1}{2}M_1(\dot{v})^2\Big|_{x=L/4} + \frac{1}{2}M_1(\dot{w})^2\Big|_{x=L/4} \\
&+ \frac{1}{2}M_1\Omega^2(v)^2\Big|_{x=L/4} + \frac{1}{2}M_1\Omega^2(w)^2\Big|_{x=L/4} \\
&+ M_1\Omega(\dot{w}v)\Big|_{x=L/4} - M_1\Omega(\dot{v}w)\Big|_{x=L/4} \\
&+ \frac{1}{2}\rho_1 hJ_{p1}\Omega^2 + \rho_1 hJ_{p1}\Omega(\dot{w}'v')\Big|_{x=L/4} \\
&+ \frac{1}{2}\rho_1 hI_1(\dot{v}')^2\Big|_{x=L/4} + \frac{1}{2}\rho_1 hI_1(\dot{w}')^2\Big|_{x=L/4} \\
&+ \frac{1}{2}\rho_1 hI_1\Omega^2(v')^2\Big|_{x=L/4} + \frac{1}{2}\rho_1 hI_1\Omega^2(w')^2\Big|_{x=L/4} \\
&+ \rho_1 hI_1\Omega(\dot{w}'v')\Big|_{x=L/4} - \rho_1 hI_1\Omega(\dot{v}'w')\Big|_{x=L/4} \\
&+ \frac{1}{2}M_2(\dot{v})^2\Big|_{x=3L/4} + \frac{1}{2}M_2(\dot{w})^2\Big|_{x=3L/4} \\
&+ \frac{1}{2}M_2\Omega^2(v)^2\Big|_{x=3L/4} + \frac{1}{2}M_2\Omega^2(w)^2\Big|_{x=3L/4} \\
&+ M_2\Omega(\dot{w}v)\Big|_{x=3L/4} - M_2\Omega(\dot{v}w)\Big|_{x=3L/4} \\
&+ \frac{1}{2}\rho_2 hJ_{p2}\Omega^2 + \rho_2 hJ_{p2}\Omega(\dot{w}'v')\Big|_{x=3L/4} \\
&+ \frac{1}{2}\rho_2 hI_2(\dot{v}')^2\Big|_{x=3L/4} + \frac{1}{2}\rho_2 hI_2(\dot{w}')^2\Big|_{x=3L/4} \\
&+ \frac{1}{2}\rho_2 hI_2\Omega^2(v')^2\Big|_{x=3L/4} + \frac{1}{2}\rho_2 hI_2\Omega^2(w')^2\Big|_{x=3L/4} \\
&+ \rho_2 hI_2\Omega(\dot{w}'v')\Big|_{x=3L/4} - \rho_2 hI_2\Omega(\dot{v}'w')\Big|_{x=3L/4}
\end{aligned} \tag{6}$$

The strain energy of the shaft as a result of bending has the form.

$$U_s = \frac{1}{2}EI_s \int_0^L \left[\left(\frac{d^2v}{dx^2}\right)^2 + \left(\frac{d^2w}{dx^2}\right)^2\right] dx \tag{7}$$

2.4. Equations of motion

To derive the equations of motion, it is convenient to use the assumed mode method and define displacements as:

$$v(x,t) = (\phi(x))^T\ q_v(t) = \phi^T(x)\,q_v(t) \tag{8}$$

$$w(x,t) = (\phi(x))^T\ q_w(t) = \phi^T(x)\,q_w(t) \tag{9}$$

The spatial function vector $\phi(x)$ characterizes the permissible transverse shaft deflections. The superscript T signifies the transpose operation applied to matrices or vectors. Furthermore, $\phi(x)$, $q_v(t)$, and $q_w(t)$ are the column vectors consisting of the corresponding time-dependent generalized coordinates.

Lagrange's equation:

The Lagrange's equations is expressed as

$$\frac{d}{dt}\left(\frac{\partial T}{\partial \dot{q}}\right) - \frac{\partial T}{\partial q} + \frac{\partial U}{\partial q} - \frac{\partial W_{\text{ext}}}{\partial q} = 0 \tag{10}$$

Lagrange's equation manipulations, results in :

$$\begin{aligned}
&\rho A\ddot{q}_v \int_0^L \phi^2\,dx + \rho I_s\ddot{q}_v \int_0^L (\phi')^2\,dx \\
&+ M_1\ddot{q}_v\phi^2\Big|_{x=L/4} + \rho_1 hI_1\ddot{q}_v(\phi')^2\Big|_{x=L/4} \\
&+ M_2\ddot{q}_v\phi^2\Big|_{x=3L/4} + \rho_2 hI_2\ddot{q}_v(\phi')^2\Big|_{x=3L/4} \\
&- 2\rho A\Omega\dot{q}_w \int_0^L \phi^2\,dx - 2\rho I_s\Omega\dot{q}_w \int_0^L (\phi')^2\,dx \\
&- 2M_1\Omega\dot{q}_w\phi^2\Big|_{x=L/4} - 2\rho_1 hI_1\Omega\dot{q}_w(\phi')^2\Big|_{x=L/4} \\
&- 2M_2\Omega\dot{q}_w\phi^2\Big|_{x=3L/4} - 2\rho_2 hI_2\Omega\dot{q}_w(\phi')^2\Big|_{x=3L/4} \\
&- \rho J_{ps}\Omega\dot{q}_w \int_0^L (\phi')^2\,dx - \rho_1 hJ_{p1}\Omega\dot{q}_w(\phi')^2\Big|_{x=L/4} \\
&- \rho_2 hJ_{p2}\Omega\dot{q}_w(\phi')^2\Big|_{x=3L/4} - \rho A\Omega^2 q_v \int_0^L \phi^2\,dx \\
&- \rho I_s\Omega^2 q_v \int_0^L (\phi')^2\,dx - M_1\Omega^2\phi^2 q_v\Big|_{x=L/4} \\
&- \rho_1 hI_1\Omega^2 q_v(\phi')^2\Big|_{x=L/4} - M_2\Omega^2\phi^2 q_v\Big|_{x=3L/4} \\
&- \rho_2 hI_2\Omega^2 q_v(\phi')^2\Big|_{x=3L/4} + EI_s q_v \int_0^L (\phi'')^2\,dx \\
&- F(t)\phi_1\Big|_{x=L/4} = 0
\end{aligned} \tag{11}$$

$$
\begin{aligned}
&\rho A \ddot{q_w} \int_0^L \phi^2 \, dx + \rho I_s \ddot{q_w} \int_0^L (\phi')^2 \, dx \\
&\quad + M_1 \ddot{q_w} \phi^2 \Big|_{x=L/4} + \rho_1 h I_1 \ddot{q_w} (\phi')^2 \Big|_{x=L/4} \\
&\quad + M_2 \ddot{q_w} \phi^2 \Big|_{x=3L/4} + \rho_2 h I_2 \ddot{q_w} (\phi')^2 \Big|_{x=3L/4} \\
&\quad - 2\rho A \Omega \dot{q_v} \int_0^L \phi^2 \, dx - 2\rho I_s \Omega \dot{q_v} \int_0^L (\phi')^2 \, dx \\
&\quad - 2M_1 \Omega \dot{q_v} \phi^2 \Big|_{x=L/4} - 2\rho_1 h I_1 \Omega \dot{q_v} (\phi')^2 \Big|_{x=L/4} \\
&\quad - 2M_2 \Omega \dot{q_v} \phi^2 \Big|_{x=3L/4} - 2\rho_2 h I_2 \Omega \dot{q_v} (\phi')^2 \Big|_{x=3L/4} \\
&\quad - \rho J_{ps} \Omega \dot{q_v} \int_0^L (\phi')^2 \, dx - \rho_1 h J_{p1} \Omega \dot{q_v} (\phi')^2 \Big|_{x=L/4} \\
&\quad - \rho_2 h J_{p2} \Omega \dot{q_v} (\phi')^2 \Big|_{x=3L/4} - \rho A \Omega^2 q_w \int_0^L \phi^2 \, dx \\
&\quad - \rho I_s \Omega^2 q_w \int_0^L (\phi')^2 \, dx - M_1 \Omega^2 \phi^2 q_w \Big|_{x=L/4} \\
&\quad - \rho_1 h I_1 \Omega^2 q_w (\phi')^2 \Big|_{x=L/4} - M_2 \Omega^2 \phi^2 q_w \Big|_{x=3L/4} \\
&\quad - \rho_2 h I_2 \Omega^2 q_w (\phi')^2 \Big|_{x=3L/4} + E I_s q_w \int_0^L (\phi'')^2 \, dx \\
&\quad = 0
\end{aligned}
\tag{12}
$$

The term Ω represents phrases concerning gyroscopic effects. These effects are crucial because they introduce coupling between transverse displacements (v and w), changing the stiffness matrix (K) to account for rotational dynamics. These terms are derived from the gyroscopic couple generated by the angular velocity Ω, which is important for proper modal analysis of rotating systems.

2.5. Equations of motion

For the assumed mode method, it can be assumed that for 1st transverse mode,

$$\phi(x) = \sin\left(\frac{\pi x}{L}\right) \tag{13}$$

$$\phi' = \frac{\pi}{L} \cos\left(\frac{\pi x}{L}\right) \tag{14}$$

$$\phi'' = -\frac{\pi^2}{L^2} \sin\left(\frac{\pi x}{L}\right) \tag{15}$$

Substituting the Eq(13), (14), and (15) into the equations (11) and (12)

A system of linear ordinary differential equations for assumed mode can be obtained as:

$$M_i \ddot{q}_{v_i}(t) - C_i \dot{q}_{w_i}(t) + K_i q_{v_i}(t) = F_i(t) \tag{16}$$

$$M_i \ddot{q}_{w_i}(t) + C_i \dot{q}_{v_i}(t) + K_i q_{w_i}(t) = 0 \tag{17}$$

where,

$$
\begin{aligned}
M_i = {} & \frac{1}{2}\rho A L + \frac{\pi^2}{2L}\rho I_S + \frac{M_1}{2} + \frac{\pi^2}{2L^2}\rho_1 h I_2 + \frac{M_2}{2} \\
& + \frac{\pi^2}{2L^2}\rho_2 h I_2
\end{aligned}
\tag{18}
$$

$$
\begin{aligned}
C_i = {} & \rho A L \Omega + \frac{\pi^2}{L}\rho I_S \Omega + M_1 \Omega + \frac{\pi^2}{L^2}\rho_1 h I_1 \Omega + \\
& \frac{\pi^2}{2L}\rho J_{PS}\Omega + \frac{\pi^2}{2L^2}\rho_1 h J_{P1}\Omega + M_G \Omega + \frac{\pi^2}{L^2}\rho_2 h I_2 \Omega \\
& + \frac{\pi^2}{2L^2}\rho_2 h J_{P2}\Omega
\end{aligned}
\tag{19}
$$

$$
\begin{aligned}
K_i = {} & \frac{\pi^4}{2L^3} E I_S - \frac{1}{2}\rho A L \Omega^2 - \frac{\pi^2}{2L}\rho I_S \Omega^2 - \frac{M_1}{2}\Omega^2 \\
& - \frac{\pi^2}{2L^2}\rho_1 h I_1 \Omega^2 - \frac{M_2}{2}\Omega^2 - \frac{\pi^2}{2L^2}\rho_2 h I_2 \Omega^2
\end{aligned}
\tag{20}
$$

$$F_i = \frac{F(t)}{2} \tag{21}$$

where,

Modal Mass (M_i): The mass associated with the i^{th} mode of vibration.

Modal Damping due to Gyroscopic Effect (C_i): The damping associated with the i^{th} mode caused by gyroscopic effects.

Modal Stiffness (K_i): The stiffness associated with the i^{th} mode.

Modal Force of the System (F_i): The external force acting on the system in the i^{th} mode.

2.6. Solution for free response of the system

For free vibration analysis, substituting F(t)=0. The natural frequencies corresponding to backward whirl and forward whirl are respectively given by:

$$
\left(\lambda_i\right)_1 = \sqrt{\frac{1}{2}\left[\left(\frac{C_i}{M_i}\right)^2 + \frac{2K_i}{M_i} - \sqrt{\left(\frac{C_i}{M_i}\right)^4 + 4\left(\frac{C_i}{M_i}\right)^2 \frac{K_i}{M_i}}\right]}
\tag{22}
$$

$$(\lambda_i)_2 = \sqrt{\frac{1}{2}\left[\left(\frac{C_i}{M_i}\right)^2 + \frac{2K_i}{M_i} + \sqrt{\left(\frac{C_i}{M_i}\right)^4 + 4\left(\frac{C_i}{M_i}\right)^2 \frac{K_i}{M_i}}\right]} \tag{23}$$

3. Modal analysis

3.1. Defining geometry

The modal analysis was conducted using a finite element analysis approach. The 3D-model was designed using CATIA V5 as it provides the ability to visualize design with ease, its disciplined system, sketching and rendering technology, Engineering insights, Multiplatform development and so on. For this research work, the system was assumed to consist of a rigid disk, flexible shaft and rigid, undamped, and simply supported bearings. The two disks were positioned along the length of the shaft, which was simply supported by bearings at both ends, spanning a total length of 2.12 meters. Each disk is situated at 450mm i.e., L/4 from the respective bearing on either side, resulting in a symmetrical arrangement. The distance between the centers of the disks is L/2, effectively dividing the shaft into two equal segments. The model designed in CATIA is shown in the Figure 3.

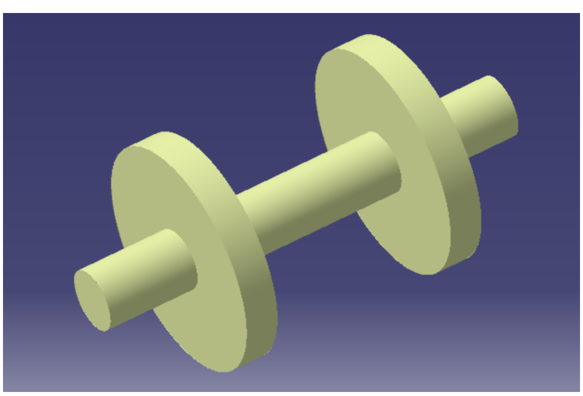

Figure 3: Assembly of Shaft-disk system designed Using CATIA

3.2. Mesh generation

The mesh was generated using ANSYS workbench default modal analysis; Mechanical APDL solver. The element order was set to be program-controlled type by setting the element size equal to 0.02m. By keeping all the default settings, the model consists of 4,32,156 nodes and 1,00,018 elements. To establish consistency, simulations were rerun with mesh sizes of 0.01m and 0.03m. The results, reported in table, reveal low fluctuation in natural frequencies, supporting mesh independence.

Natural frequency and deviation for different mesh sizes and speeds

Mesh Size (m)	Speed (rad/s)	Natural Frequency (Hz)	Deviation
0.01	0	65.02	3.18%
0.01	100	73.16	1%
0.01	200	92.54	2.31%
0.01	300	112.04	1.8%
0.01	400	124.98	0.31%
0.01	500	141.68	0.68%
0.02	0	67.155	Reference
0.02	100	72.437	Reference
0.02	200	94.736	Reference
0.02	300	110.051	Reference
0.02	400	125.380	Reference
0.02	500	140.723	Reference
0.03	0	66.49	1%
0.03	100	72.91	0.65%
0.03	200	93.501	1.30%
0.03	300	111.531	1.35%
0.03	400	126.67	1.02%
0.03	500	141.35	0.45%

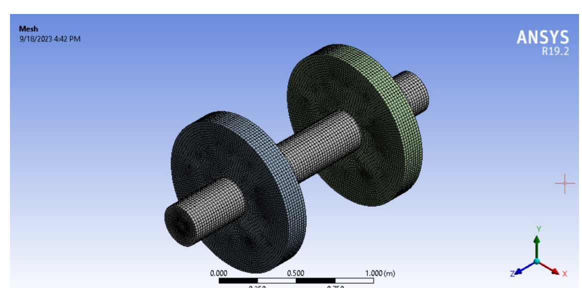

Figure 4: Mesh Generation

3.3. Model setup

The simulation's material for the model configuration was stainless steel. The simulation's boundary conditions were simply supported by a bearing at the shaft's end. With 100 rad/s intervals, the assembly's rotational velocity was varied from 0 to 500 rad/s about the Z-axis.

4. Results and discussion

To facilitate a comparison between the mathematical model and simulation results, we have selected specific parameters and computed them, as illustrated in Table 1.

Table 1: Parameters of the Shaft and Disks for Euler Bernouli model

Parameter	Value	Units
Density of Shaft material, ρ	7750	Kg/m^3
Density of Disk 1 material, ρ_1	7750	Kg/m^3
Density of Disk 2 material, ρ_2	7750	Kg/m^3
Length of the shaft, L	2.12	m
Cross-sectional area of shaft, A	0.066	m^2
Modulus of Elasticity of shaft and disk material, E	1.93×10^{11}	Pa
Thickness of Disks, h	0.16	m
Area moment of inertia of the shaft section, I_s	3.472×10^{-4}	m^4
Area moment of inertia of the disk 1, I_1	0.0642	m^4
Area moment of inertia of the disk 2, I_2	0.0642	m^4
Polar moment of area of the shaft, J_{ps}	6.944×10^{-4}	m^4
Polar moment of area of the disk 1, J_{p1}	0.129	m^4
Polar moment of area of the disk 2, J_{p2}	0.129	m^4
Mass of Disk 1, M_1	1035.2	Kg
Mass of Disk 2, M_2	1035.2	Kg

Using Equations (18), (19), and (20), the Equivalent Mass (M_i), Equivalent Damping Coefficient (C_i), and Stiffness (K_i) for the first mode of transverse vibration are found and tabulated in Table 2.

Table 2: Equivalent parameters for the first mode

Equivalent Parameters	First Mode	Units
Mass (M_i)	1758.48	Kg
Damping Coefficient (C_i)	3880.74	N.s/m
Stiffness (K_i)	342530255-1758.47	N.m

The natural frequencies corresponding to backward whirl and forward whirl were found using equations (25) and (26). These values are tabulated in given Table 3.

Table 3: Natural frequency corresponding to BW and FW

Spin Speed (Ω) (rad/s)	BW Frequency (λ_1) (Hz)	FW Frequency (λ_2) (Hz)
0	70.24	70.24
100	53.20	88.11
200	38.13	106.41
300	28.33	124.93
400	29.68	143.59
500	41.05	162.35

The results obtained from the modal analysis are illustrated in Campbell's diagram in Figure 5 . For the First mode of transverse vibration, mode stability was found to be stable with a critical velocity of 459.83rad/s. The natural frequency corresponding to the first mode of transverse vibration of the system obtained from the modal analysis were tabulated in Table 4.

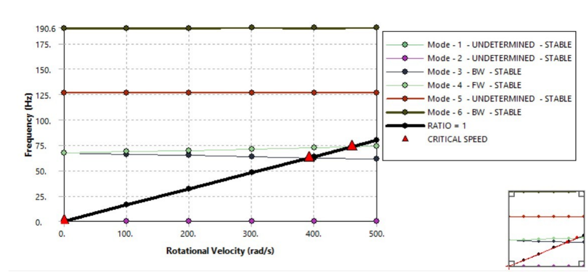

Figure 5: Campbell diagram generated from ANSYS

Table 4: Natural frequency corresponding to first mode of transverse vibration obtained computationally

Spin Speed (Ω) (rad/s)	Forward Whirl Natural Frequency (λ) (Hz)
0	67.155
100	72.437
200	94.736
300	110.051
400	125.380
500	140.723

The mathematical model and simulation successfully validated the natural frequency of the first mode of transverse vibration, demonstrating their consistency and accuracy.

5. Conclusion

In this study, a rotating Euler-Bernoulli Beam model is used to investigate the dynamic behaviour of a multi-rotor system. In this model for bending vibrations in transverse motion, the governing equations are identified as a coupled system of differential equations.

Through a comprehensive free vibration analysis, critical speeds of the system for an operational speed of omega = 500 rad/s are determined for the first transverse mode within the Euler- Bernoulli beam model. The critical speeds are found to be 162.35 Hz for a forward whirl and 41.05 Hz for a backward whirl. Modal analysis using ANSYS reveals critical speeds of 140 Hz for a forward whirl and 55.21 Hz.

Subsequent steps following the research could involve a sensitivity analysis to gain insights into how the system reacts to changes in parameters, conducting experimental validation to verify the analytical and numerical results, implementing structural improvements guided by the critical speed findings, sharing research outcomes through publication and knowledge dissemination, utilizing the research findings for educational purposes, and investigating opportunities for interdisciplinary applications to incorporate the research into interconnected fields.

Acknowledgement

The authors would like to express their appreciation to the Department of Mechanical and Aerospace Engineering for generously providing access to a workspace and a well-equipped digital manufacturing facility. Additionally, the authors extend their gratitude to Er. Madhav Baral and Er. Sanjeev Karki for their unwavering technical assistance throughout the research endeavors.

References

[1] Luintel M. Dynamic modelling and response of a pelton turbine unit[D]. Ph. D. Thesis, Lalitpur, Nepal, 2019.

[2] Chen X, Zhai J, Zhang H, et al. Simulation study on unbalance vibration characteristics of dual-rotor system[J]. SN Applied Sciences, 2020, 2: 1-24.

[3] Timsina R, Luitel M C. Dynamic response of vertical shaft pelton turbine unit for free vibration[C]// Proceedings of IOE Graduate Conference: volume 8. 2020: 164-170.

[4] Dukkipati V R, Srinivas J. Textbook of mechanical vibrations[M]. PHI Learning Pvt. Ltd., 2012.

[5] Kushwaha N, Patel V. Nonlinear dynamic analysis of two-disk rotor system containing an unbalance influenced transverse crack[J]. Nonlinear Dynamics, 2023, 111(2): 1109-1137.

[6] Karki S, Luintel M C, Poudel L. Dynamic response of pelton turbine unit for forced vibration[C]// IOE Graduate Conference. 2017.

[7] Meirovitch L. Principles and techniques of vibrations[M]. 1997.

[8] Khanlo H, Ghayour M, Ziaei-Rad S. Chaotic vibration analysis of rotating, flexible, continuous shaft-disk system with a rub-impact between the disk and the stator[J]. Communications in Nonlinear Science and Numerical Simulation, 2011, 16(1): 566-582.